CERES_EBAF-Surface_Ed4.0

Data Quality Summary (May 26, 2017)

Investigation: **CERES**
Data Product: **EBAF-Surface**

Data Set: **Terra (Instruments: CERES-FM1 or CERES-FM2)**
Aqua (Instruments: CERES-FM3 or CERES-FM4)

Data Set Version: **Edition4.0** **Release Date: May 26, 2017**

Subsetting Tool Availability: http://ceres.larc.nasa.gov

The purpose of this document is to inform users of the accuracy of this data product as determined by the CERES Science Team. The document summarizes key validation results, provides cautions where users might easily misinterpret the data, provides links to further information about the data product, algorithms, and accuracy, and gives information about planned data improvements.

This document provides a high-level quality assessment of the CERES EBAF-Surface data product that contains surface fluxes consistent with the top-of-atmosphere fluxes contained in the CERES Energy Balanced and Filled (EBAF-TOA) data product. As such, this document represents the minimum information needed by scientists for appropriate and successful use of the CERES EBAF-Surface data product. For a more thorough description of the methodology used to produce EBAF-Surface, please see Kato et al. (2013). It is strongly suggested that authors, researchers, and reviewers of research papers re-check this document for the latest status before publication of any scientific papers using this data product.

Changes from EBAF-Surface Ed2.8:

- Ed4 EBAF-surface uses a consistent source of temperature and humidity throughout for the entire time record.
- Ed4 EBAF-surface uses MODIS collection 5 for the entire time record. As aconsequence, there is no significant discontinuity in the time series of clear-sky downward shortwave flux anomalies over land.
- Surface longwave longwave fluxes are improved because of the improvement of nighttime retrieved cloud properties.

NOTE: To navigate the document, use Bookmarks in Adobe Reader.
Select "View > Show/Hide > Navigation Panes > Bookmarks."

TABLE OF CONTENTS

Section Page

LIST OF FIGURES

Figure Page

LIST OF TABLES

Table Page

1.0 Introduction

In order to determine the distribution of surface radiation over the globe, the CERES team relies on radiative transfer model calculations initialized using satellite-based cloud and aerosol retrievals and meteorological and aerosol assimilation data from reanalysis to characterize the atmospheric state. The accuracy and stability in computed top-of-atmosphere (TOA) and surface fluxes thus depend upon the quality of the input cloud and atmospheric data (e.g. Rose et al. 2013). The standard CERES data products (e.g., SYN1deg-Month) use cloud and aerosol properties derived from MODIS radiances, meteorological assimilation data from the Goddard Earth Observing System (GEOS) Version 5.4.1 model, and aerosol assimilation from the Model for Atmospheric Transport and Chemistry (MATCH; Collins et al. 2001).

In order to minimize the error in surface fluxes due to uncertainties in the input data sources, the EBAF-Surface data product introduces several additional constraints based upon information from other independent data sources, such as CERES TOA fluxes, AIRS-derived temperature/humidity profiles, and CALIPSO/CloudSat-derived vertical profiles of clouds.

This document describes the procedure used to determine EBAF surface fluxes and provides an assessment of the uncertainty of the EBAF-Surface product.

2.0 Description

Surface fluxes in EBAF-Surface are derived from three CERES data products: (i) CERES SYN1deg-Month (Doelling et al. 2013; Rutan et al. 2015) Ed4 provides computed surface fluxes to be adjusted, (ii) CERES EBAF-TOA Ed4.0 (Loeb et al. 2009, Loeb et al. 2012, Loeb et al. 2016) provides the CERES-derived TOA flux constraints by observations, and iii) SYN1deg-Hour provides weightes to compute monthly mean computed clear-sky TOA fluxes.

SYN1deg-Month is a Level 3 product and contains gridded monthly mean computed TOA and surface fluxes along with fluxes at four atmospheric pressure levels (70, 200, 500, and 850 hPa). Surface fluxes in SYN1deg-Month are computed with cloud properties derived from MODIS and geostationary satellites (GEO), where each geostationary satellite instrument is calibrated against MODIS (Doelling et al. 2013). The Ed4 CERES cloud algorithm (Minnis et al. 2016) derives cloud properties (e.g. fraction, optical depth, top height, and particle size) from narrowband radiances measured by MODIS, twice a day from March 2000 through August 2002 (Terra only) and four times a day after September 2002 (Terra plus Aqua). The Edition 4 multi-channel GEO cloud algorithm (Mecikalski et al. 2007; Minnis et al. 2001) provides cloud properties (fraction, top height, optical depth, phase, particle size) every one hour between Terra and Aqua observations. Cloud properties are gridded onto a 1°×1° spatial grid and1 hourly intervals (hour boxes). Although it occurs less frequently than Ed2.8, cloud properties are missing in some hour boxes. Missing cloud properties are estimated by interpolating nearlest hour boxes. Up to four cloud-top heights (cloud types, high, mid-high, mid-low, and low) are retained for each hour box within a 1°×1° grid box. Cloud properties (cloud top height, optical thickness, particle size, phase etc.) are kept separately for four cloud types.

To treat horizontal variability of optical thickness within a cloud type explicitly, both linear and logarithmic means of the cloud optical thicknesses are computed for each cloud type. The distribution of cloud optical thickness expressed as a gamma distribution is estimated from the linear and logarithmic cloud optical thickness means (Barker 1996; Oreopoulos and Barker 1999; Kato et al. 2005). Once the distribution of cloud optical thickness is estimated for each cloud type, a gamma-weighted two-stream radiative transfer model (Kato et al. 2005), when the shape factor is less than 10, otherwise a four-stream model is used to compute the shortwave flux vertical profile for each cloud type. The logarithmic mean optical thickness is used in the longwave flux computation with a modified 2-stream approximation (Toon et al. 1989; Fu et al. 1997). The cloud base height, which largely influences the surface downward longwave flux in midlatitude and polar regions, is estimated by an empirical formula described by Minnis et al. (2016).

Temperature and humidity profiles used in the radiative transfer model calculations are from the Goddard Earth Observing System (GEOS-5.4.1) Data Assimilation System reanalysis (Rienecker et al. 2008). Although the GEOS-5.4.1 product has a higher temporal and spatial resolutions, 6 hourly 1°×1° GEOS-5.4.1 temperature and relative humidity profiles are used for surface computations. Skin temperatures used in the computations are a 3-hourly resolution. Column ozone amount is also taken from GEOS-5.4.1. Other inputs used in SYN1deg-Month include ocean spectral surface albedo from Jin et al. (2004). Broadband land surface albedos are inferred

from the clear-sky TOA albedo derived from CERES measurements (Rutan et al. 2009). In addition, MODIS spectral radiances over partly cloudy scenes are used to estimate surface albedo over the clear-sky part of partly cloudy scenes. Emissivity is based on Wilber et al. (1999). Aerosol optical thickness are from an aerosol transport model MATCH (Collins et al. 2001) that assimilates and spatially and temporally interpolates MODIS aerosol optical thickness.

The spectral solar constant used in the shortwave radiative transfer code is Newkur taken from MODTRAN. The solar constant integrated over the entire solar spectral is normalized to match observation provided by the Solar Radiation and Climate Experiment (SORCE) Total Solar Irradiance (TSI) V-15 dataset.

Computed TOA fluxes from SYN1deg-Month do not necessarily agree with the CERES-derived TOA fluxes from EBAF-TOA Ed4.0, partly because of the error in inputs used in the computations and, to a smaller extent, due to assumption in the radiative transfer model. To minimize the error in surface fluxes, we use an objective contain by a Lagrange multiplier algorithm to adjust surface, atmospheric, and cloud properties within their uncertainties in order to ensure that computed TOA fluxes are consistent with the CERES-derived TOA fluxes within their observational errors. The steps involved in the process are follows:

- Determine 1°×1° monthly mean differences between the computed TOA fluxes from SYN1deg-Month and the fluxes from CERES EBAF-TOA.
- Correct the TOA longwave bias error caused by the upper tropospheric relative humidity and temperature errors in GEOS-5.4.1 using AIRS (AIRX3STM.006) data. A minor correction also applied to the clear-sky downward longwave flux. We correct the bias error of the surface downward longwave flux, which is caused by the error in cloud fraction viewed from the surface. In addition, we correct TOA shortwave and longwave, as well as downward and upward surface shortwave fluxes due to the error in the space view cloud fraction. These bias corrections due to surface and space view cloud fractions are based upon the difference between CALIPSO/CloudSat, MODIS and geostationary satellite derived cloud fraction.
- Use a Lagrange multiplier procedure to determine the perturbation of surface, cloud, and atmospheric properties to match the TOA flux differences, assuming that perturbations applied to the input variables are small relative to their respective monthly mean values. Jacobians that are needed to determine surface, cloud, and atmospheric property perturbations, as well as surface flux adjustments, are computed separately and used in the Lagrange multiplier procedure.
- Compute the surface flux change based on these perturbed surface, cloud, and atmospheric properties. Subsequently, the surface flux changes are added to the 1°×1° monthly mean Ed4 SYN1deg-Month fluxes.

2.1 All-sky Surface Flux

Monthly mean all-sky surface shortwave and longwave fluxes for 1°×1° grids are computed by averaging hourly Ed4 SYN1deg all-sky fluxes. We compare monthly 1°×1° TOA shortwave and longwave fluxes with those from EBAF-TOA and compute the difference. Based on the differences, we adjust monthly 1°×1° upward and downward shortwave and longwave fluxes. As

mentioned in the precious section, multiple steps are involved in the process to adjust surface fluxes. Processes are separated into two groups, bias corrections and Lagrange multiplier. We first correct biases to reduce the difference of computed and EBAF TOA shortwave and longwave fluxes before Lagrange multiplier is used. The bias correction also mitigates TOA flux differences to be attributed to atmospheric and cloud properties incorrectly by Lagrange multiplier.

2.1.1 Bias correction

Inputs used for computing SYN1deg fluxes are mostly based on observations. When input variables are compared with observations taken by different instruments or derived from other algorithms, some input variables differ significantly. For example, GEOS-5.4.1 upper tropospheric specific humidity is much larger than upper tropospheric specific humidity derived from AIRS. In addition, when thin clouds are screened out, the cloud fraction derived from MODIS and GEOs are larger than the cloud fraction derived from CALIPSO and CloudSat. A larger upper tropospheric specific humidity reduces computed TOA longwave fluxes and a larger cloud fraction increases computed TOA shortwave fluxes. The difference between SYN computed and EBAF TOA fluxes are consistent with these biases. Therefore, correcting these biases reduces the difference of computed and EBAF TOA longwave and shortwave fluxes. CALIPSO and CloudSat also provide the occurrence of lower-level clouds present underneath upper-layer clouds that are difficult to observe by MODIS and GEOs. Including lower level clouds in computing surface fluxes is especially critical for accurate surface downward longwave flux estimates because the downward longwave flux is sensitive to the cloud base height and TOA fluxes does not provide a strong constraint on the surface downward longwave flux.

In summary, we consider the bias in temperature (T) and specific humidity (q) between the 200 hPa and 500 hPa levels, cloud fraction viewed from space, and cloud fraction viewed from the surface in the bias correction process. Fluxes adjusted by these bias correction processes are listed in Table 2-1.

All-sky and clear-sky radiative kernels are derived from Ed4 SYN1deg with a temporal resolution of 3 hourly and spatial resolution of 1°×1° using 2008 data (Thorsen et al. 2017). The interannual variability of kernels is negligible. We average kernels over a month but maintain the spatial resolution of 1°×1°. Cloud kernels are computed 4 different cloud types (high, mid-high, mid-low, and low) separately.

Table 2-1. Fluxes adjusted in the bias correction process.

Bias correction process	Adjusted fluxes	Resolution and type
Temperature (T) and specific humidity (q) between the 200 hPa and 500 hPa	Clear-sky and all-sky TOA upward longwave fluxes Clear-sky surface downward longwave flux	1°×1°, ocean and land
Cloud fraction viewed from space	All-sky TOA upward shortwave and longwave fluxes All-sky surface upward and downward shortwave fluxes	1°×1°, ocean
Cloud fraction viewed from the surface	All-sky surface downward longwave flux	1degree zonal with 5 degree smoothing, land and ocean

2.1.1.1 Bias in upper tropospheric Temperature (T) and specific humidity (q)

The bias correction of T and q between 200 hPa and 500 hPa is based on the difference of those from GEOS-5.4.1. and derived from AIRS. Although AIRS T and q are not necessarily correct, they are derived from observed TOA spectral radiances. Correcting GEOS-5.4.1 T and q toward those derived from AIRS makes TOA spectral radiance more consistent with observations, if spectral radiances were computed. The bias is estimated by comparing monthly mean 1°×1° GEOS-5.4.1 T and q in 100 hPa layers between 300 hPa and 500 hPa and 50 hPa layers between 200 hPa and 300 hPa with those from the AIRS level3 version 6 product (AIRX3STM.006, TqJoint grid product). We convert the difference (GEOS-5.4.1 – AIRS) of T and q, layer by layer, to the difference of all-sky and clear-sky TOA longwave fluxes using all-sky and clear-sky radiative kernels. In addition, the surface downward longwave flux is also corrected using clear-sky radiative kernel. Radiative kernels are built by regionally and monthly with no year to year variation (i.e. same regional kernel for January of different years). Computed clear-sky TOA longwave and surface fluxes are subsequently corrected. All-sky surface downward longwave flux is not corrected in this process but it is corrected separately.

AIRS observations are not available before September 2002. We use climatological differences of GEOS-5.4.1 and AIRS monthly 1°×1° T and q between 200 hPa and 500 hPa derived from 14 years of data (from September 2000 through August 2015). Similarly, we use climatological clear-sky radiative kernel to convert T and q differences to TOA longwave and surface downward longwave fluxes. Therefore, TOA longwave and surface downward longwave from March 2000 through August 2002 are adjusted using their monthly 1°×1° climatological adjustments derived from September 2000 through August 2015.

2.1.1.2 Bias in the cloud fraction viewed from space

The bias correction of all-sky TOA shortwave and longwave fluxes and surface downward shortwave fluxes caused by the bias in the cloud fraction viewed from the space involves cloud fraction derived by CALIPSO, CloudSat, MODIS, and GEOs. We correct only low-level cloud fractions over ocean because regions with a larger difference between computed and observed TOA shortwave irradiances are coincide with regions where low-level clouds are often present. In addition, a comparison of cloud fractions derived from MODIS and CALIPSO/CloudSat by

cloud type also indicates that the Ed4 MODIS cloud algorithm overestimates the low-level cloud fraction. A further analysis shows that Ed4 GEO cloud algorithms overestimate the low cloud fraction over oceans compared to the low-level cloud fraction derived by the Ed4 MODIS cloud algorithm.

We first estimate the difference of the zonal cloud fraction over ocean derived from MODIS on Aqua and CALIPSO/CloudSat. MODIS cloud fraction is derived over CERES footprints that include the CALIPSO/CloudSat ground track. Therefore, the viewing zenith angle of MODIS is near nadir. Clouds with optical thickness less than 0.3 are excluded from both cloud fractions derived from MODIS (using MODIS-derived optical thickness) and CALIPSO/CloudSat (using CALIPSO-derived extinction profile). We then derive the zonal cloud fraction relative difference (CC-MODIS(A))/TAG, including all cloud types, where CC indicates the cloud fraction derived from CALIPSO/CloudSat, TAG (TAGi in Figure 2-1) indicates cloud fraction derived from Terra MODIS+Aqua MODIS+GEOs, and MODIS(A) is Aqua only. When all cloud types are included, the global mean relative cloud fraction difference averaged over 4 months (January, April, July, and October 2010) (CC-MODIS)/TAG is -6.7%, i.e. the MODIS-derived cloud fraction is generally larger than CC. We include all cloud types in comparing MODIS and CALIPSO/CloudSat because, when high- and low-level clouds overlap, MODIS tends to retrieve low-level clouds while the upper-most cloud layer derived from CALIPSO/CloudSat is high-level clouds. A part of the low-level cloud fraction derived from MODIS and CALIPSO/CloudSat is caused by the different instrument footprint sizes. Our further study indicates that the difference in the footprint size leads to the difference in the global mean water cloud fraction difference of about 0.02.

Second, we compute zonal low-level cloud fraction derived from Terra MODIS, Aqua MODIS, and GEOs using seasonal months (January, April, July, and October 2010). We then compute relative zonal cloud fraction difference of Terra, Aqua, and GEOs combined (TAG) to Terra plus Aqua, (TAG-MODIS (T&A))/TAG (thick black line in Figure 2-1). The global mean relative low-level cloud fraction difference is -6.0%, i.e. GEO derived cloud fraction is generally larger than MODIS derived cloud fraction.

Third, we simply add these two relative zonal cloud fraction differences to come up with the zonal relative cloud fraction bias correction, which is indicated by the thick purple line ((CC-MODIS(A))/TAG + (TAG-MODIS (T&A))/TAG) in Figure 2-1. The global mean relative difference is -12.7%. We multiply 1°×1° monthly mean low-level cloud fraction over ocean by this relative zonal cloud fraction difference to compute the 1°×1° monthly low-level cloud fraction bias. We then use 1°×1° monthly cloud fraction kernels computed with Ed4 SYN1deg clouds to convert the cloud fraction bias to TOA shortwave and longwave flux and surface downward shortwave flux biases.

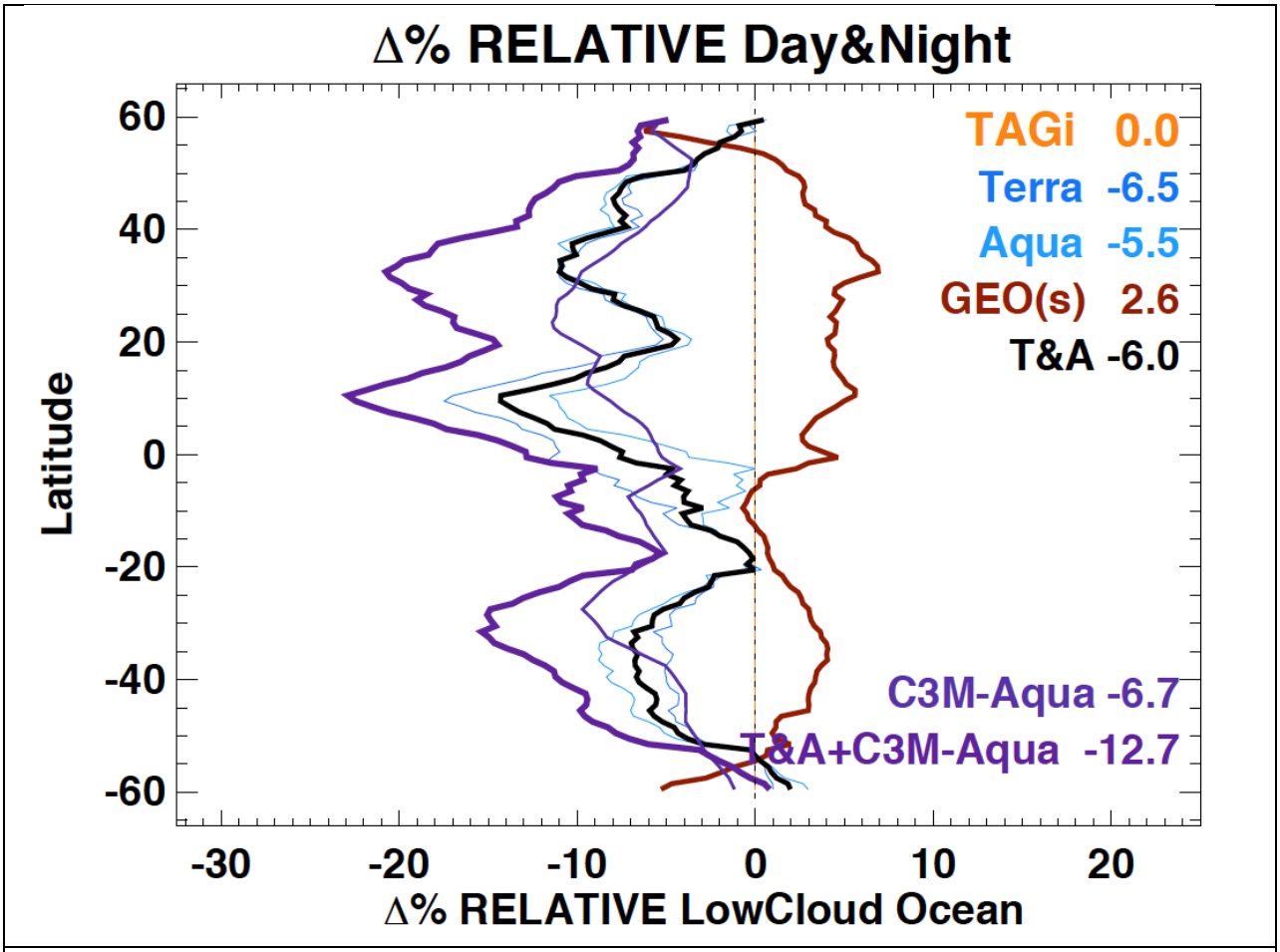

Figure 2-1. Relative difference of zonal day plus night cloud fraction from the cloud fraction derived from Terra MODIS + Aqua MODIS+ Geostationary satellites (TAGi). Thin blue lines and thick black line indicate the zonal cloud fraction derived from, respectively, Terra or Aqua MODIS and Terra and Aqua MODIS combined, and thick black line is thick red line indicated zonal cloud fraction derived from geostationary satellites (GEOs). Thin purple line is the cloud fraction difference (CALIPSO/CloudSat minus Aqua MODIS) divided by TAGi. The thick purple line is the sum of thick black line and thin purple line, which is the relative cloud fraction bias error by TAGi.

2.1.1.3 Bias in the cloud fraction viewed from the surface

The bias of the surface downward longwave flux is estimated with cloud fraction viewed from the surface. In addition to 4 cloud types (high, high-high, mid-low, and low), Ed4 SYN considers lower-level clouds with a random cloud overlap assumption. This results in the total of 16 different single and two overlapping layer combinations. However, only four most frequently occurring cloud layer combinations are used in computing surface fluxes in Ed4 SYN for a given 1°×1° grid and an hour box. Using 4 most frequent occurring cloud layer combinations used in Ed4 SYN, we compute zonal cloud fraction viewed from the surface over ocean and land. Similarly, we compute zonal cloud fraction viewed from the surface from CALIPSO/CloudSat data. We exclude clouds with optical thickness less than 0.3 and CALIPSO CAD score less than 70. Monthly zonal mean surface view cloud fraction difference over ocean and land separated by

cloud type at a 1 degree resolution with 5-degree smoothing is computed using data from January to December 2008. We then convert the bias in zonal monthly mean low-level cloud fraction viewed from the surface (surface view cloud fraction multiplied by relative zonal surface view cloud fraction bias) to the bias in the monthly zonal surface downward longwave flux using zonal cloud fraction kernels derived with Ed4 SYN1deg clouds. Summing up the monthly zonal surface downward longwave flux computed four cloud types, we obtain the zonal monthly bias correction for land and ocean separately.

2.1.2 Lagrange Multiplier

Inputs to the Lagrange multiplier algorithm are modeled and EBAF shortwave and longwave TOA flux differences and their uncertainties. Other inputs are estimated uncertainties of selected input variables used for SYN flux computations.

TOA longwave flux change due to the bias in upper tropospheric T and q and TOA shortwave and longwave flux changes due to the bias in the space view cloud fraction discussed in Section 2.1.1 are subtracted from the difference of Ed4 SYN and EBAF-TOA fluxes. We correct the bias of TOA fluxes monthly and regionally (1°×1°). Uncertainties used in the Lagrange multiplier process are shown in Table 2-2 and Table 2-3**.** Partial derivatives of TOA and surface fluxes with respect to atmospheric, cloud, and surface properties (Jacobians) are calculated with monthly mean values with a spatial scale of a 1°×1°. Jacobians are calculated for clear-sky and all-sky separately.

Table 2-2. All-sky and clear-sky TOA and surface flux1σ uncertainties for 1°×1° monthly flux adjustment.

Flux	Uncertainty (1σ)
TOA Shortwave (Wm^{-2})	0.5
TOA Longwave (Wm^{-2})	0.5
Surface Downward Shortwave	1° Zonal RMS difference of Ed4 and Ed3 monthly fluxes[1]
Surface Upward Shortwave	1° Zonal RMS difference of Ed4 and Ed3 monthly fluxes[1]
Surface Downward Longwave	1° Zonal RMS difference of Ed4 and Ed3 monthly fluxes[1]
Surface Upward Longwave	1° Zonal RMS difference of Ed4 and Ed3 monthly fluxes[1]

[1]12 seasonal months separated by ocean, land, and cryosphere, all-sky and clear-sky derived based on 2008 to 2011 data.

Table 2-3. All-sky and clear-sky 1σ uncertainties of surface, atmospheric, and cloud properties for 1°×1° monthly flux adjustment.

Variable	Uncertainty (1σ)
Skin temperature[1]	Monthly 1°×1° AIRS – GEOS-5.4.1 absolute difference
Surface air temperature[1]	Monthly 1°×1° AIRS – GEOS-5.4.1 absolute difference
Upper tropospheric relative humidity[1]	Monthly 1°×1° AIRS – GEOS-5.4.1 absolute difference
Precipitable water[1]	Monthly 1°×1° AIRS – GEOS-5.4.1 absolute difference
Aerosol optical thickness (relative)	Ocean: 15%, Land: 10%, Cryosphere: 10%
Surface albedo (relative)	Ocean: 1%, Land: 4%, Cryosphere: 8%
Cloud fraction (absolute)	0.05
Cloud optical thickness (relative)	15%
Cloud top pressure (hPa)	10
Cloud base pressure (hPa)	10

[1] Uncertainty value varies depending on month and 1°×1° region.

2.2 Clear-sky Surface Flux

The bias correction and Lagrange multiplier process for clear-sky is the same as those for all-sky processes. The clear-sky flux adjustment involves an additional process to make the sampling of computed fluxes to be consistent with observed clear-sky fluxes. Monthly mean clear-sky surface shortwave and longwave fluxes $\langle F \rangle$ are computed by averaging daily hourly Ed4 SYN1deg clear-sky fluxes (i.e. averaging hourly fluxes of the same hour in a day over a month) that computed by removing clouds weighted by the clear fraction over a 1°×1° grid box to form monthly mean hourly fluxes and averaging monthly hourly fluxes,

$$\langle F \rangle = \frac{1}{n_{hour}} \sum_{i=1}^{n_{hour}} \frac{\sum_{j=1}^{n_{day}} w_{ij} F_{ij}}{\sum_{j=1}^{n_{day}} w_{ij}},$$

where w_{ij} is the clear fraction at i-th hour on j-th day in the month, and F_{ij} is either hourly mean shortwave or longwave fluxes. For longwave fluxes, $\langle F_{LW} \rangle = \langle F \rangle$. For shortwave irradiances, the insolation correction ratio $\langle R \rangle$ is computed by,

$$\langle R \rangle = \frac{\sum_{i=1}^{n_{hour}} \sum_{j=1}^{n_{day}} F_{0,ij} / (n_{day} n_{hour})}{\sum_{i=1}^{n_{hour}} \sum_{j=1}^{n_{day}} w_{ij} F_{0,ij} / \left(n_{hour} \sum_{j=1}^{n_{day}} w_{ij} \right)},$$

where F_0 is the solar constant and $\langle F_{SW} \rangle = \langle R \rangle \langle F \rangle$. The clear-sky fraction is derived from MODIS. The cloud fraction for hour boxes with no MODIS observations are derived by interpolating MODIS-derived clear fraction.

Clear-sky TOA longwave and surface downward longwave flux bias due to upper tropospheric temperature and specific humidity is corrected by the process explained in Section 2.1 (All-sky surface flux).

2.3 EBAF-Surface Ed4.0 Improvements over EBAF-Surface Ed2.8

Ed4 EBAF-surface uses a consistent source of temperature and humidity throughout the time series. Using GEOS-5.4.1 for the entire record improves anomaly time series of surface flux significantly compared to Ed2.8. Specifically, the trend in anomaly time series of net longwave flux over ocean, land and polar regions is significantly reduced.

In Ed 2.8, MODIS Collection 4 is switched to Collection 5 at the end of March 2006. The switch caused a shift in the retrieved aerosol optical thickness over land. In Ed4, collection 5 is used for the entire record. As a consequence, the trend in the anomaly time series of clear-sky surface downward shortwave flux is significantly smaller in Ed4 EBAF-surface.

Ed2 GEO cloud algorithm only uses two channels (one visible and one IR). Although geostationary satellites with only two channels are still used in Ed 4, up to 5 channels for other geostationary satellites are used in the Ed4 GEO cloud algorithm. As a consequence, nighttime retrieved cloud properties (e.g. particle size, top pressure, phase) are improved significantly.

Because the clear-sky sampling in EBAF-TOA is improved, unphysical cloud radiative effects, such as frequency of occurrence of a negative surface net longwave cloud radiative effect or a positive surface net shortwave cloud radiative effect, are reduced.

3.0 Cautions and Helpful Hints

The CERES Science Team notes several CAUTIONS and HELPFUL HINTS regarding the use of CERES_EBAF-Surface_Ed4.0:

- The CERES_EBAF-Surface_Ed4.0 product can be visualized, subsetted, and ordered from: (http://ceres.larc.nasa.gov).
- The CERES team has significantly reduced GEO artifacts in CERES_EBAF-Surface_Ed4.0 as compared to surface fluxes included in SYN1deg-Month for two reasons. The GEO-derived cloud fraction errors are corrected based on the cloud fraction derived from CALIPSO and CloudSat, and computed fluxes at TOA are constrained by CERES EBAF-TOA.
- CERES_EBAF-Surface_Ed4.0 does not contain TOA fluxes. The corresponding TOA fluxes are included in CERES_EBAF-TOA_Ed4.0.
- Clear-sky surface fluxes are consistent with clear-sky TOA fluxes included in CERES-EBAF-TOA_Ed4.0. Therefore, the monthly 1°×1° gridded clear-sky fluxes are clear-sky fraction-weighted fluxes instead of fluxes computed by removing clouds. Computed clear-sky fluxes are also constrained by the CERES-derived clear-sky TOA fluxes that are included in CERES_EBAF-TOA_Ed4.0.
- Global means are determined using zonal geodetic weights. The zonal geodetic weights can be obtained from (http://ceres.larc.nasa.gov/science_information.php?page=GeodeticWeights).
- Cloud radiative effects are computed as all-sky flux minus clear-sky flux.
- The net flux is positive when the energy is deposited to the surface, i.e. the net is defined as downward minus upward flux.
- There are regions where the surface flux adjustments are large, such as over the Andes, Tibet, and central eastern Africa. As a result, the deseasonalized anomalies over these regions can be noisy.
- Because of the degradation of Terra water vapor chanles that affects cloud retrievals starting around 2008, downward longwave flux anomalies over polar regions shows downward trend (see Section 4.5). Therfore, trend analyses with surface fluxes over polare regions from Ed4 EBAF-surface should be avoided.
- The climatological mean values are calculated relative to a base period of July 2005 – June 2015.

Surface fluxes

Even though we do not explicitly match the sampling of clear-sky with clear-sky sampling of EBAF-TOA, the adjustment process force the sampling of clear-sky EBAF-surface nearly equal to the sampling of clear-sky EBAF-TOA. Therefore, clear-sky surface fluxes differ from clear-sky surface fluxes computed by removing clouds. Clear-sky scenes tend to occur when the atmosphere is dryer than all-sky atmospheric conditions. In addition, in some regions, aerosol loading for clear-sky scenes tends to be less than aerosol loading for all-sky conditions.

Although the frequency of occurrence of a positive net shortwave cloud effect and a negative net longwave cloud effect is reduced, they are not entirely absent. A possible reason that these

apparently unphysical cloud radiative effects occur is because of a mismatch of sampling between all-sky and clear-sky. For example, if clear-sky is sampled during daytime more often than during nighttime, the net clear-sky longwave flux is less negative than the net clear-sky longwave flux with a uniform sample throughout a month. Therefore, when the less negative clear-sky net longwave flux is subtracted from all-sky net longwave flux, which is also generally negative, the resulting net longwave cloud effect can be negative. For shortwave over polar region where the solar zenith angle changes rapidly over the course of a month, if clear-sky samplings occur when solar zenith angle is large and a smaller net clear-sky shortwave flux is subtracted from all-sky net shortwave flux, the cloud effect can be positive.

Cloud properties

Cloud properties distributed with EBAF-TOA are not cloud properties used for surface flux computations in SYN1deg. While Terra and Aqua MODIS instruments observe 4 times a day for a given region, cloud properties in other 20 hour boxes between 60°N and 60°S are derived from GEOs. Therefore, cloud properties included in Ed4 SYN are more closely related to EBAF-surface fluxes than cloud properties distributed with EBAF-TOA. Surface fluxes from EBAF-surface over regions poleward from 60° are computed with cloud properties distributed with EBAF-TOA. However, bias correction and Lagrange multiplier processes alter cloud properties that are used in flux computations so that resulting cloud properties differ from those from SYN1deg and provided by EBAF-TOA. The result of altered cloud properties are not provided.

A larger number of inputs are required in deriving surface fluxes compared to the number of inputs used for deriving TOA fluxes. In addition, surface fluxes are computed with input variables, unlike TOA fluxes that are derived directly from radiance observations. As a consequence, surface fluxes are more vulnerable to artifacts present in input data. It is hard to determine whether a specific large surface flux anomaly is real or caused by artifacts. If it is caused by artifacts, it is even harder to determine what variables are responsible for the artifact. But the standard deviation of deseasonalized anomalies and standard deviation of the difference of surface fluxes of two consecutive months are useful metrics to detect artifacts. The size of flux anomalies depends on spatial and temporal scales. Usually, a visual inspection of anomaly time series is enough to detect large anomalies. To make a quantitative decision, we provide two sets of standard deviations in Table 3-1 and Table 3-2. If one finds a flux anomaly larger than standard deviations with a similar temporal and spatial scale shown in Table 3-1 and Table 3-2, one should be cautious treating the anomaly or computing a trend with the anomaly. These values do not tell if the anomalies are real or artifacts. Anomalies greater than these values, however, need to have physical reasons for the large magnitude.

Table 3-1. Standard deviation of deseasonalized anomalies of fluxes averaged over three surface types in W m^{-2}. Numbers in parentheses are in percentage of the standard deviation relative to the mean.

	Global	Ocean	Land	Polar
All-sky				
SW down	0.78 (0.42)	1.00 (0.53)	1.35 (0.69)	1.83 (1.54)
SW up	0.29 (1.21)	0.22 (1.79)	0.54 (1.46)	2.20 (2.56)
LW down	1.07 (0.31)	1.02 (0.28)	1.69 (0.51)	2.91 (1.58)
LW up	0.78 (0.20)	0.66 (0.16)	1.45 (0.37)	2.68 (1.22)
Clear-sky				
SW down	0.50 (0.21)	0.55 (0.22)	0.80 (0.32)	1.07 (0.74)
SW up	0.34 (1.12)	0.26 (1.51)	0.68 (1.47)	2.37 (2.38)
LW down	1.01 (0.32)	0.90 (0.27)	1.70 (0.55)	2.05 (1.43)
LW up	0.78 (0.20)	0.68 (0.16)	1.44 (0.36)	2.70 (1.24)

Table 3-2. Standard deviation of the flux anomaly difference between two consecutive months averaged over three surface types in W $m^{-2.}$

	Global	Ocean	Land	Polar
All-sky				
SW down	0.91 (0.48)	1.25 (0.66)	1.75 (0.90)	2.09 (1.75)
SW up	0.24 (1.02)	0.17 (1.35)	0.56 (1.52)	1.95 (2.28)
LW down	0.59 (0.17)	0.55 (0.15)	1.38 (0.41)	3.67 (2.00)
LW up	0.42 (0.11)	0.21 (0.05)	1.34 (0.34)	3.26 (1.49)
Clear-sky				
SW down	0.48 (0.20)	0.55 (0.22)	0.84 (0.34)	1.24 (0.85)
SW up	0.28 (0.92)	0.21 (1.21)	0.68 (1.46)	2.23 (2.24)
LW down	0.50 (0.16)	0.41 (0.12)	1.41 (0.46)	2.49 (1.74)
LW up	0.42 (0.11)	0.23 (0.05)	1.38 (0.35)	3.06 (1.41)

4.0 Accuracy and Validation

Uncertainties in surface fluxes at various temporal and special scales are estimated by Kato et al. (2013). In this section, we update uncertainty given in Kato et al. (2013) with surface fluxxes from Ed4 EBAF-surface.

4.1 Regional mean all-sky surface fluxes

We assume that the random error is caused by uncertainties in the variables shown in Table 2-3. The bias correction made due to the estimated bias in upper tropospheric relative humidity and cloud fraction viewed from space and surface is treated as a 1σ uncertainty. In addition, the uncertainties shown in Table 2-3 that are used in Lagrange multiplier are treated as random 1σ errors. We convert these uncertainties to surface irradiance uncertainties using radiative kernels. All components are assumed to be independent.

We compare the uncertainty calculated from uncertainty in input variables with the RMS error of computed and observed surface fluxes (Table 4-1). We will use the larger value for a given surface type (e.g. land, ocean, Arctic, and Antarctic) as the uncertainty.

Table 4-1. Uncertainty in regional (1°×1°) monthly mean irradiances

	Shortwave (Wm^{-2})		Longwave (Wm^{-2})	
	Downward	Upward	Downward	Upward
Ocean	11	1	5	5
Land	12	4	10	18
Arctic (60°N-90°N)	14	6	12	12
Antarctic (60°S-90°S)	21	24	12	13

4.2 Validation by surface observations

Figure 4-1 shows the difference of EBAF monthly 1°×1° mean surface (top) shortwave and (bottom) longwave downward fluxes from observed fluxes at buoys (computed minus observed). The mean difference on monthly mean fluxes averaged for 49 buoy sites is 4.9 Wm^{-2} for downward shortwave and 1.1 Wm^{-2} for downward longwave with the standard deviation of, respectively, 10.5 Wm^{-2} and 4.7 Wm^{-2}. Larger differences over tropical Atlantic ocean is caused by accumulation of dusts transported from Africa on buoys (Foltz et al. 2013). The bias of downward shortwave flux can exceed -40 Wm^{-2} in a monthly mean for buoys located in the high-dust region (8°, 12°, and 15°N along 38°W; 12° and 21°N along 23°W), while mean bias is of the order of -10 Wm^{-2}.

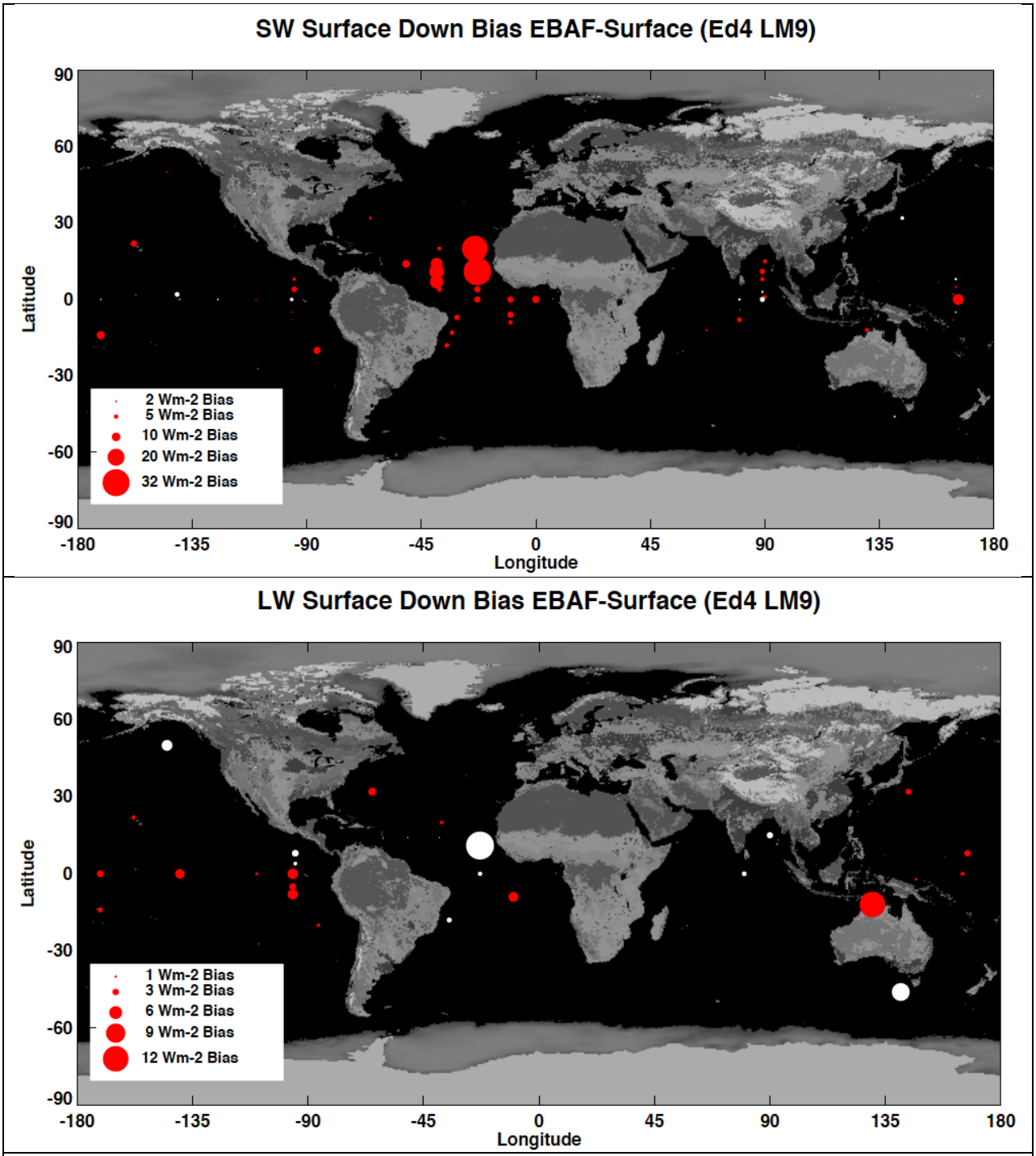

Figures under 201706 (mapbuoyerr.*.pdf)

Figure 4-1. Difference of EBAF monthly 1°×1° mean surface (top) shortwave and (bottom) longwave downward fluxes from observed fluxes at buoys (computed minus observed). The size of the circle is proportional to the difference. The red and white circles indicate, respectively, a positive and a negative difference. The number of months used for comparisons varies depending on buoys.

Comparisons with surface observations by surface type are shown in Table 4-2**.** Buoys in the tropical Atlantic ocean that have large biases due to African dust are excluded in computing the statistics shown in here.

Table 4-2. Difference in EBAF surface monthly 1°×1° mean downward shortwave and longwave fluxes (W m^{-2}) from surface observations. Numbers in parentheses are the standard deviations.

	Downward Shortwave	Downward Longwave
All sites (85 sites)	1.98 (12.64)	0.08 (9.21)
Ocean buoys	4.67 (10.65)	1.19 (4.84)
Land	-0.74 (11.59)	0.04 (9.76)
Arctic	3.74 (13.15)	0.43 (12.34)
Antarctic	-4.07 (20.13)	3.14 (11.73)

4.3 Comparison at Greenland sites

Downward surface shortwave fluxes are biased negative by 4 W m^{-2} and Downward surface longwave fluxes are biased positive by 11 W m^{-2} compared with observation taken at the Summit (SMT) (Figure 4-2). This is primarily due to a positive bias of cloud fraction over high elevation regions. In particular, low-mid and high-mid cloud fractions are biased high over the Summit site except for summer time. The effect of the positive bias of cloud fraction on surface radiative fluxes for other polar regions is less pronounced (Table 4-1).

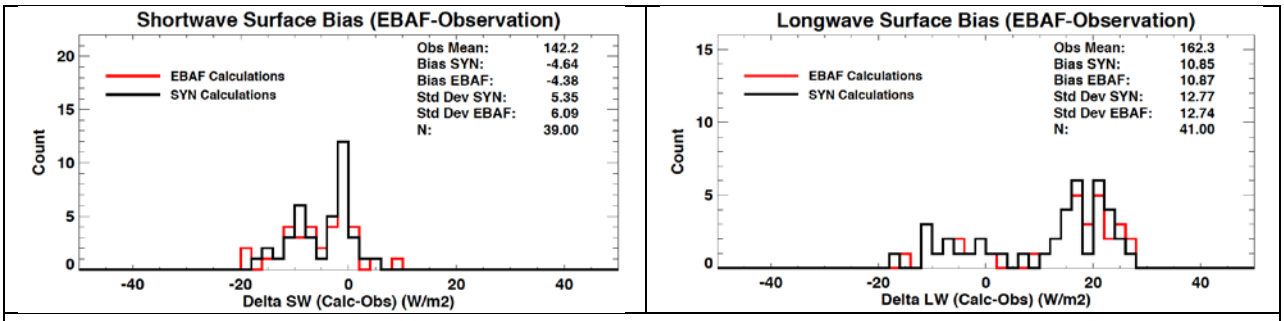

Figure 4-2. Histogram of computed minus observed monthly mean downward shortwave (left) and downward longwave (right) fluxes over the Greenland Summit site. Observed data are provided by Nate Miller.

4.4 Surface longwave flux during polar nights

Because of the degradation of Terra MODIS water vapor channel that is used to detect clouds mostly at high altitude in polar regions during polar nights, the nighttime cloud fraction over Antarctica derived from Terra MODIS is about 2% less than the nighttime cloud fraction derived from Aqua MODIS over the same region. The effect of the degradation on the surface downward

longwave flux becomes apparent around 2008. A large drop of cloud fraction derived from Terra MODOS over the Antarctica occurs March 2016. The mitigation of the impact of downward longwave flux over cryosphere will be implemented in Ed 4.1. Ed 4.1 will be released in the future.

Becsue of the degradation of the Terra water vapor channel, the time series of downward longwave flux anomalies and net longwave flux animalies over polar region (60N to 90N and 60S to 90S) shows downward trend (Figuyre 4-4). For this reason, trend analyses with surface fluxes over polare regions from Ed4.0 EBAF-surface should be avoided.

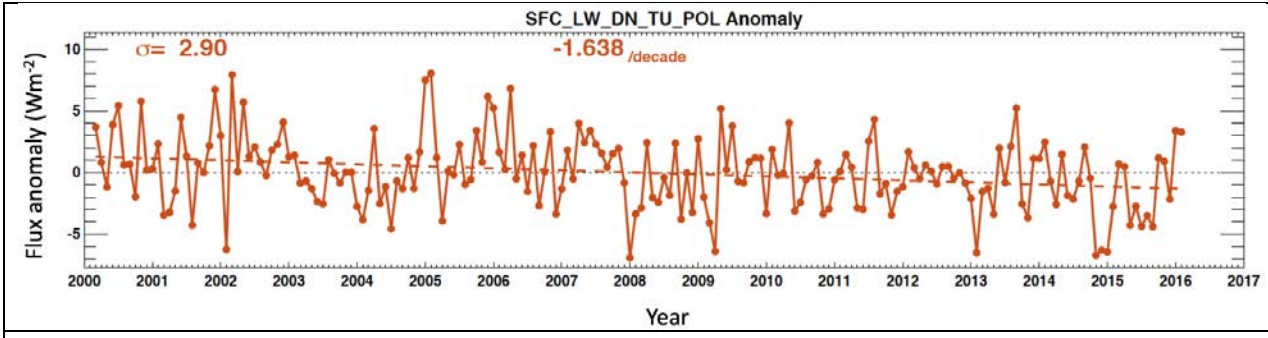

Figure 4-3. Time series of downward longwave flux anomalies over the Arctic (60°N - 90°N) and Antarctic (60°S – 90°S).

5.0 Version History Summary

5.1 Difference between EBAF Ed4.0 and EBAF Ed2.8

Differences between EBAF Ed4 and Ed2.8 are primarily caused by input differences, such as cloud properties, temperature and humidity profiles, surface albedo, and aerosol.

5.1.1 Global mean surface flux comparisons

Table 5-1. Global mean surface fluxes in W m^{-2} computed from EBAF Ed4.0 and EBAF Ed2.8 for March 2000-February 2016. compares the global mean surface fluxes from Ed 4 and Ed 2.8.

Table 5-1. Global mean surface fluxes in W m^{-2} computed from EBAF Ed4.0 and EBAF Ed2.8 for March 2000-February 2016.

All-sky	Ed4	Ed2.8	Ed4 – Ed2.8
TOA SW insolation	340.0	339.9	0.17
SW down	187.0	186.5	0.57
SW up	23.4	24.1	-0.76
SW net[1]	163.7	162.3	1.33
LW down	345.0	345.2	-0.18
LW up	398.3	398.3	0.07
LW net[1]	-53.4	-53.1	-0.25
SW+LW net	110.3	109.2	1.08
Clear-sky			
TOA SW insolation	340.0	339.9	0.17
SW down	243.7	244.1	-0.33
SW up	29.8	29.7	0.07
SW net[1]	213.9	214.3	0.41
LW down	314.1	316.3	-2.20
LW up	397.6	398.4	-0.81
LW net[1]	-83.5	-82.1	1.39
SW+LW net[1]	130.4	132.2	-1.80

[1] Net is computed by downward – upward.

5.1.2 Regional mean surface flux comparisons

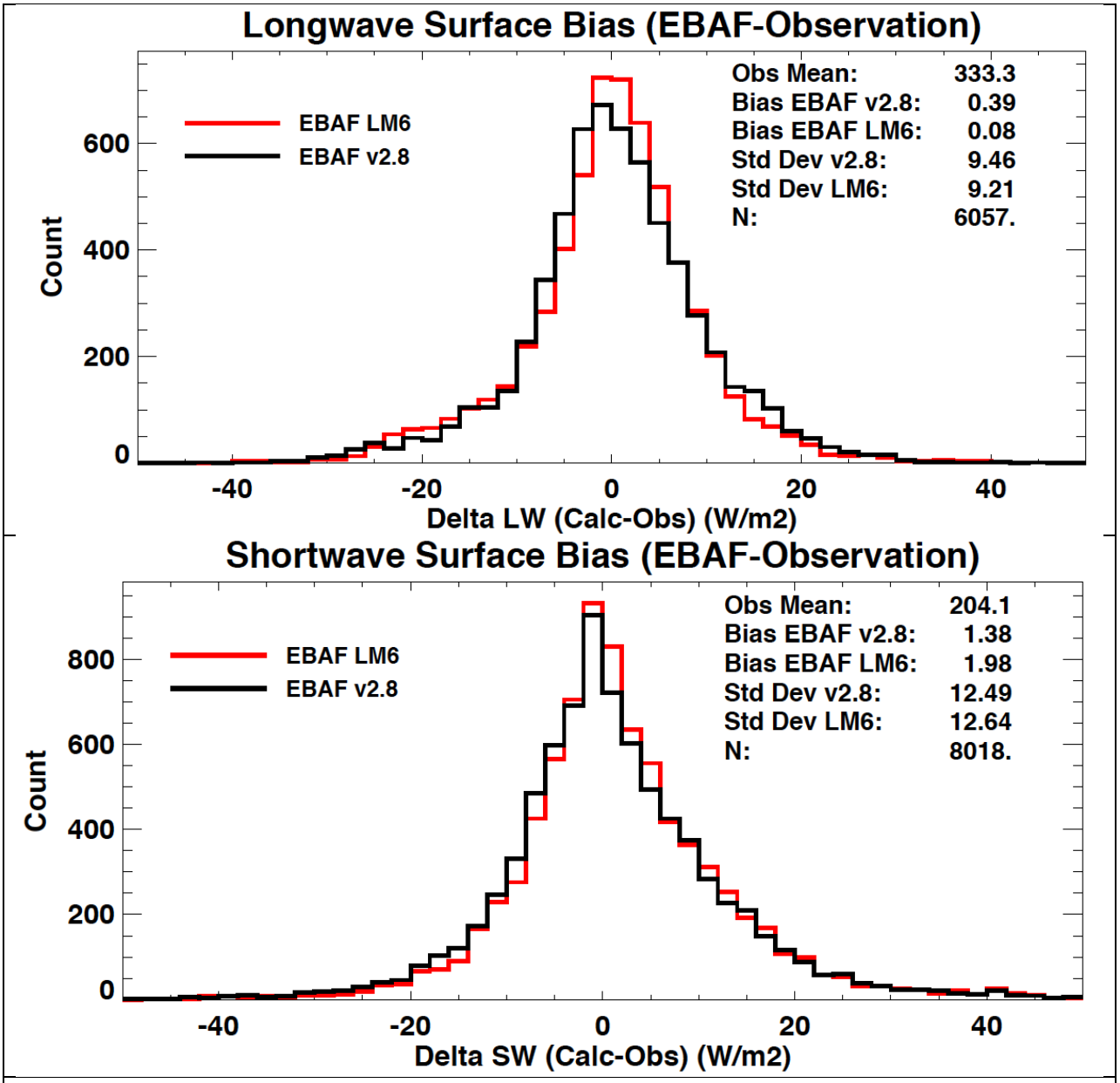

Figure 5-1. all.ebf.hist.3n4.pdf.
Histogram of computed minus observed monthly mean downward (top) shortwave and (bottom) longwave fluxes over 85 sites including 36 land sites and 49 buoys.

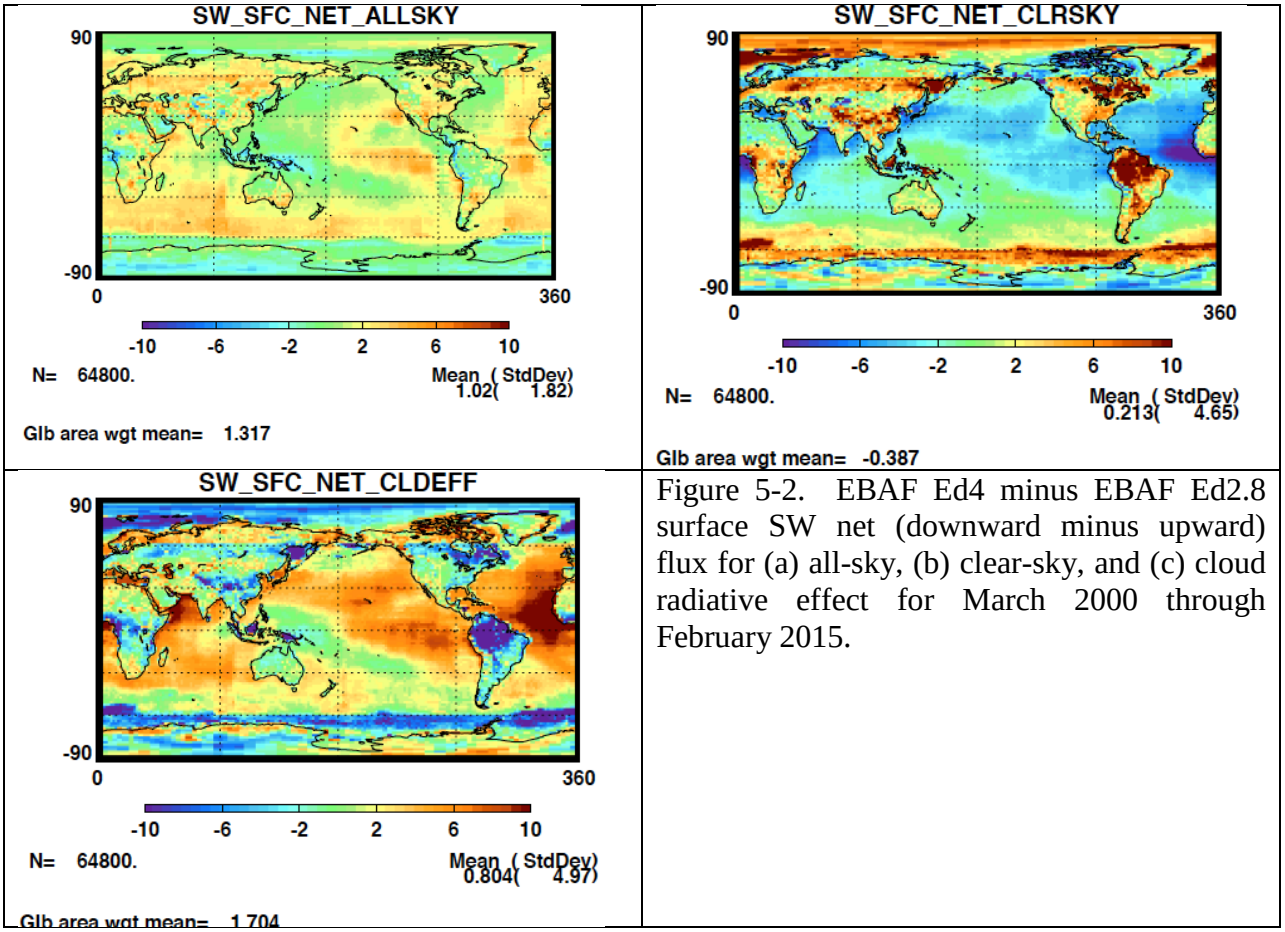

Figure 5-2. EBAF Ed4 minus EBAF Ed2.8 surface SW net (downward minus upward) flux for (a) all-sky, (b) clear-sky, and (c) cloud radiative effect for March 2000 through February 2015.

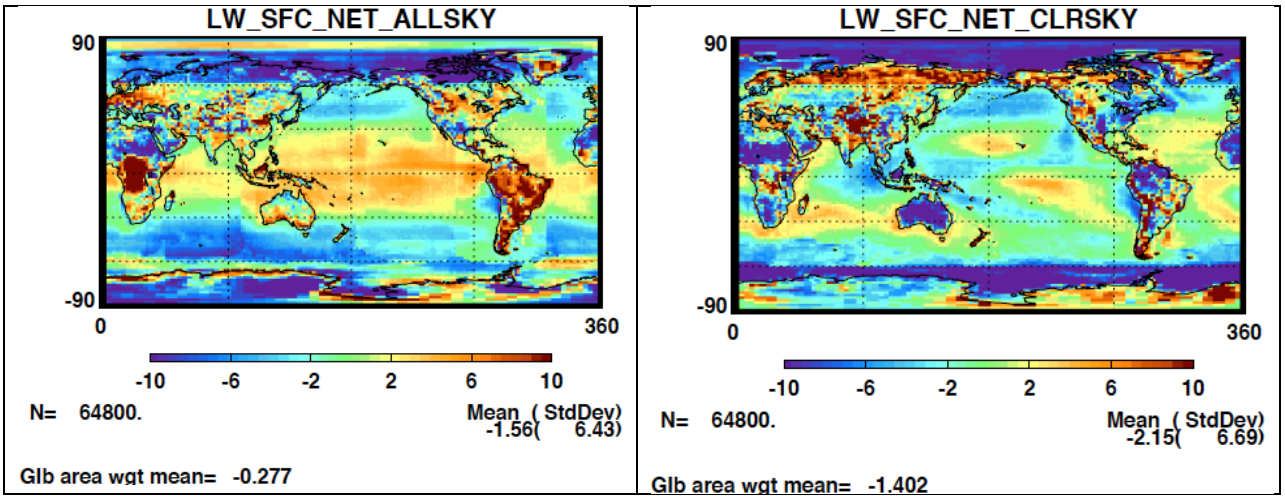

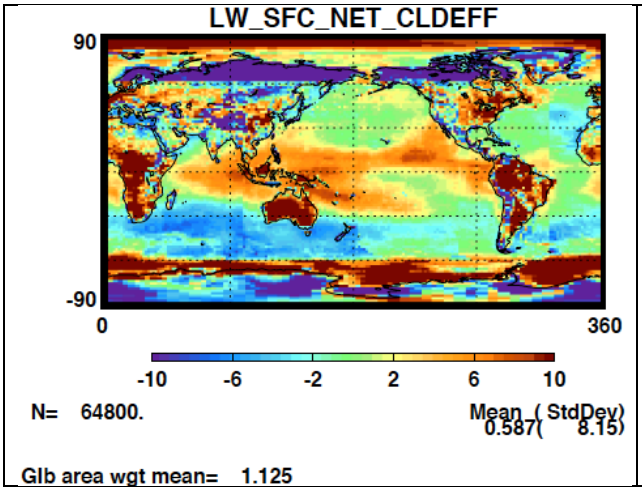

Figure 5-3. EBAF Ed4 minus EBAF Ed2.8 surface LW net (downward minus upward) flux for (a) all-sky, (b) clear-sky, and (c) cloud radiative effect for March 2000 through February 2015.

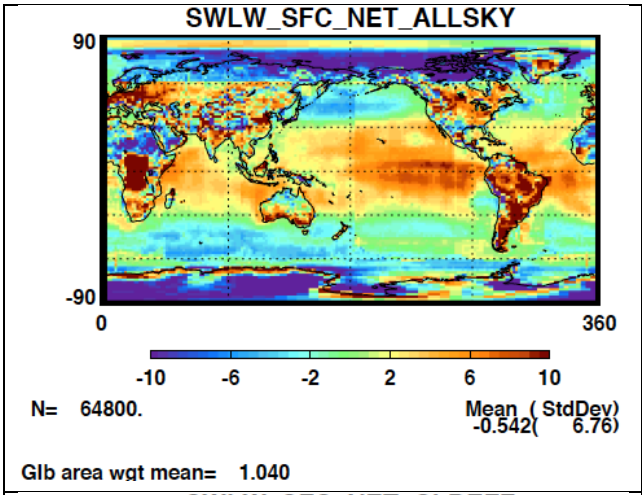

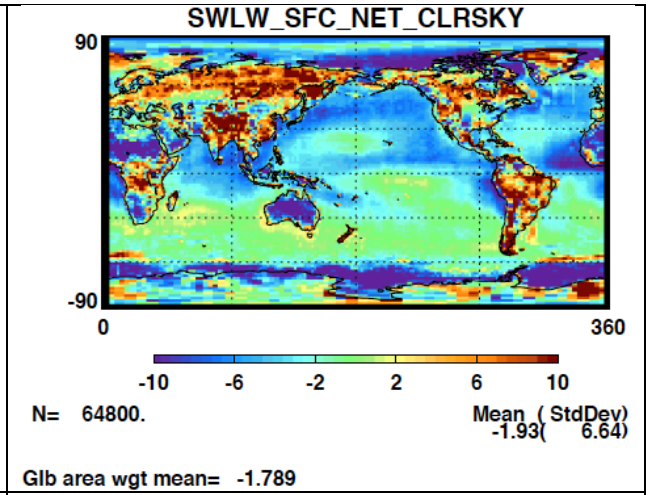

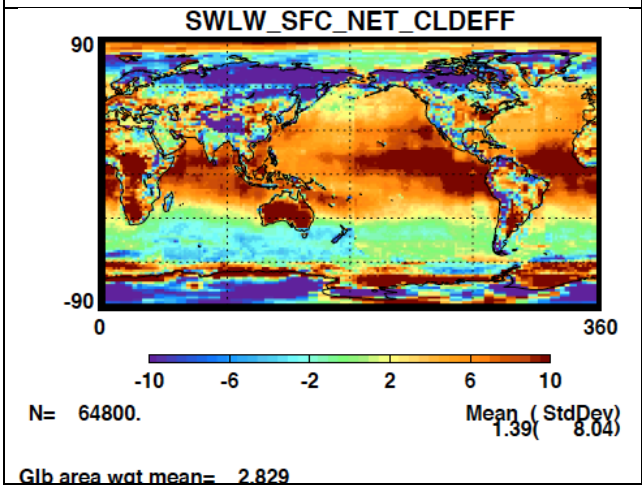

Figure 5-4. EBAF Ed4 minus EBAF Ed2.8 surface SW+LW net (downward minus upward) flux for (a) all-sky, (b) clear-sky, and (c) cloud radiative effect for March 2000 through February 2015.

6.0 References

Barker, H. W., 1996: A parameterization for computing grid-averaged solar fluxes for inhomogeneous marine boundary layer clouds. Part I: Methodology and homogeneous biases. *J. Atmos. Sci.*, 53, 2289-2303.

Collins, W. D., P. J. Rasch, B. E. Eaton, B. V. Khattatov, J.-F. Lamarque, and C. S. Zender, 2001: Simulating aerosols using a chemical transport model with assimilation of satellite aerosol retrievals: Methodology for INDOEX. *J. Geophys. Res.*, 106, 7313–7336.

Doelling, D. R., N. G. Loeb, D. F. Keyes, M. L. Nordeen, D. Morstad, C. Nguyen, B. A. Wielicki, D. F. Young, and M. Sun, 2013: Geostationary enhanced temporal interpolation for CERES flux products, *J. Atmos. Oceanic Technol.*, 30, 1072-1090, doi:10.1175/JTECH-D-12-00136.1.

Foltz, G. R., A. T. Evan, H. P. Freitag, S. Brown, M. McPhaden, 2013: Dust accumulation biases in PIRATA shortwave radiation records, J. Atmos. Ocean. Tech., 30, DOI: 10.1175/JTECH-D-12-00169.1.

Fu, Q., K. Liou, M. Cribb, T. Charlock, and A Grossman, 1997: On multiple scattering in thermal infrared radiative transfer. *J. Atmos. Sci*., 54, 2799-2812.

Jin, Z., T. P. Charlock, W. L. Smith, Jr., and K. Rutledge, 2004: A look-up table for ocean surface albedo. *Geophys. Res. Lett*., 31, L22301.

Kato, S., F. G. Rose, and T. P. Charlock, 2005: Computation of domain-averaged irradiance using satellite derived cloud properties. *J. Atmos. Oceanic Technol*., 22, 146-164.

Kato, S., N. G. Loeb, F. G. Rose, D. R. Doelling, D. A. Rutan, T. E. Caldwell, L. Yu, and R. A. Weller, 2013: Surface irradiances consistent with CERES-derived top-of-atmosphere shortwave and longwave irradiances, *J. Climate*, 26, 2719-2740, doi:10.1175/JCLI-D-12-00436.1.

Loeb, N. G., B. A. Wielicki, D. R. Doelling, G. L. Smith, D. F. Keyes, S. Kato, N. Manalo-Smith, and T. Wong, 2009: Toward optimal closure of the Earth's top-of-atmosphere radiation budget. *J. Climate*, 22, 748-766.

Loeb, N. G., J. M. Lyman, G. C. Johnson, R. P. Allan, D. R. Doelling, T. Wong, B. J. Soden, and G. L. Stephens, 2012: Observed changes in top-of-the-atmosphere radiation and upper-ocean heating consistent within uncertainty. *Nat. Geosci*., 5, 110-113. doi:10.1038/NGEO1375.

Loeb, G. N., and co-authors, 2017: Clouds and the Earth's Radiant Energy System (CERES) Energy Balance and Filled (EBAF) Edition 4.0 data product, submitted to J. Climate.

Mecikalski, J. R., and Coauthors, 2007: Aviation applications for satellite-based observations of cloud properties, convective initiation, in-flight icing, turbulence, and volcanic ash. *Bull. Amer. Meteor. Soc.*, **88**, 1589–1607.

Minnis, P., and Coauthors, 2001: A near real time method for deriving cloud and radiation properties from satel- lites for weather and climate studies. *Proc. 11th Conf. Satellite Meteorology and Oceanography,* Madison, WI, Amer. Meteor. Soc., 477–480.

Oreopoulos, L. and H. W. Barker, 1999: Accounting for subgrid-scale cloud variability in a multi-layer 1D solar radiative transfer algorithm. *Quart. J. Roy. Meteor. Soc*. 125, 301-330.

Rienecker, M. M. and Coauthors, 2008: The GOES-5 Data Assimilation System-Documentation of Versions 5.0.1, 5.1.0, and 5.2.0. NASA Tech. Rep. NASA/TM-2009-104606, Vol. 27, 118 pp.

Rose, F., D. A. Rutan, T. P. Charlock, G. L. Smith, and S. Kato, 2013: An algorithm for the constraining of radiative transfer calculations to CERES-observed broadband top-of-atmosphere irradiance, *J. Atmos. Oceanic Technol*., 30, 1091-1106, doi:10.1175/JTECH-D-12-00058.1.

Rutan, D., F. Rose, M. Roman, N. Manalo-Smith, C. Schaaf, and T. Charlock, 2009: Development and assessment of broadband surface albedo from Clouds and the Earth's Radiant Energy System clouds and radiation swath data product. *J. Geophys. Res*., 114, D08125, doi:10.1029/2008JD010669.

Toon, O. B., C. P. Mckay, T. P. Ackerman and K. Santhanam, 1989: Rapid calculation of radiative heating rates and photodissociation rates in inhomogeneous multiple scattering atmospheres. *J. Geophys. Res*., 94, 16 287–16 301.

Wilber, A. C., D. P. Kratz, and S. K. Gupta, 1999: Surface emissivity maps for use in satellite retrievals of longwave radiation. NASA Tech. Memo. TP-1999-209362, 30 pp.

7.0 Attribution

When referring to the CERES EBAF-Surface product, please include the data set version and the data product as “CERES EBAF-Surface_Ed4.0.”

The CERES Team has put forth considerable effort to remove major errors and to verify the quality and accuracy of this data. Please provide a reference to the following paper when you publish scientific results with the

CERES EBAF-Surface_Ed4.0

Kato, S., N. G. Loeb, F. G. Rose, D. R. Doelling, D. A. Rutan, T. E. Caldwell, L. Yu, and R. A. Weller, 2013: Surface irradiances consistent with CERES-derived top-of-atmosphere shortwave and longwave irradiances. *J. Climate*, 26, 2719-2740, doi:10.1175/JCLI-D-12-00436.1.

When CERES data that are obtained via the CERES web site are used in a publication, we request the following acknowledgment be included: "These data were obtained from the NASA Langley Research Center CERES ordering tool at (http://ceres.larc.nasa.gov/)."

8.0 Feedback and Questions

For questions or comments on the CERES EBAF-Surface Data Quality Summary, please contact Dr. Seiji Kato, seiji.kato@nasa.gov. For questions about the CERES subsetting/visualization/ordering tool at http://ceres.larc.nasa.gov/order_data.php, please email ceres-help@lists.nasa.gov.